Design of Annulated Pyrazoles as Inhibitors of HIV-1 Reverse Transcriptase[‖]

Zachary K. Sweeney,*,[†] Seth F. Harris,*,[‡] Nidhi Arora,[†] Hassan Javanbakht,[§] Yu Li,[⊥] Jennifer Fretland,[#] James P. Davidson,[◆] J. Roland Billedeau,[†] Shelley K. Gleason,[†] Donald Hirschfeld,[†] Joshua J. Kennedy-Smith,[†] Taraneh Mirzadegan,[†] Ralf Roetz,[†] Mark Smith,[†] Sarah Sperry,[†] Judy M. Suh,[†] Jeffrey Wu,[†] Stan Tsing,[‡] Armando G. Villaseñor,[‡] Amber Paul,[§] Guoping Su,[§] Gabrielle Heilek,[§] Julie Q. Hang,[⊥] Amy S. Zhou,[#] Jesper A. Jernelius,[◆] Fang-Jie Zhang,[◆] and Klaus Klumpp[⊥]

Departments of Medicinal Chemistry, Discovery Sciences and Technologies, Viral Disease Biology, Viral Disease Biochemistry, Non-Clinical Safety, and Chemical Synthesis, Roche Palo Alto LLC, 3431 Hillview Avenue, Palo Alto, California 94304

Non-nucleoside reverse transcriptase inhibitors (NNRTIs) are recommended components of preferred combination antiretroviral therapies used for the treatment of HIV. These regimens are extremely effective in suppressing virus replication. Structure-based optimization of diaryl ether inhibitors led to the discovery of a new series of pyrazolo[3,4-*c*]pyridazine NNRTIs that bind the reverse transcriptase enzyme of human immunodeficiency virus-1 (HIV-RT) in an expanded volume relative to most other inhibitors in this class. The binding mode maintains the β13 and β14 strands bearing Pro236 in a position similar to that in the unliganded reverse transcriptase structure, and the distribution of interactions creates the opportunity for substantial resilience to single point mutations. Several pyrazolopyridazine NNRTIs were found to be highly effective against wild-type and NNRTI-resistant viral strains in cell culture.

Introduction

Non-nucleoside reverse transcriptase inhibitors bind to an induced hydrophobic pocket adjacent to the polymerase active site of HIV-reverse transcriptase and prevent the progression of DNA synthesis from the viral RNA template.[1] Clinical studies have demonstrated that therapy with a combination of NNRTIs[a] and nucleoside or nucleotide reverse transcriptase inhibitors is able to provide a sustained reduction of viral replication in treatment-naive patients.[2] Nevertheless, a single nucleotide mutation in the HIV-genome can produce a virus that is highly resistant to NNRTIs, and treatment failure is often accompanied by the emergence of resistant viruses.[3] Many research groups have therefore attempted to discover new NNRTIs that inhibit commonly observed NNRTI-associated resistant viruses and that have a higher genetic barrier to resistance.[4−6]

Binding of NNRTIs to HIV-RT is thought to restrict the motion of key residues in the polymerase active site and prevent incorporation of nucleotides into the DNA chain during reverse transcription.[7] The reverse transcriptase enzyme is very flexible, and lead optimization using structure-based drug design and computational analysis of ligand affinity is complicated by the dynamic nature of the induced ligand binding site.[8−10] Relative to the apo enzyme, NNRTI-bound reverse transcriptases show large conformational adjustments in backbone positions and side chain rotamers, particularly of Tyr181, Tyr183, and Tyr188, that create the NNRTI pocket (Figure 1).[11,12] This induced

Chart 1. NNRTIs Efavirenz, Etravirine, and Trovirdine, Highlighting the Aniline Motif

efavirenz   etravirine   trovirdine
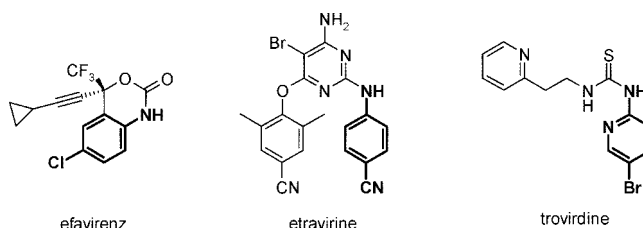
conformation also maintains a remarkable degree of plasticity, as the geometry and volume of the final protein pocket are sensitive to the shape and properties of the bound ligand.

All NNRTIs form direct or water-mediated hydrogen bonds with the protein backbone of lysine residue Lys101 or Lys103.[13] Inhibitors that maintain hydrogen bond interactions with Lys101 include efavirenz,[14] etravirine,[15] and trovirdine[16] (Chart 1). In structures of most smaller K101-binding inhibitors, strands β13 and β14 (residues 232−241) are displaced relative to their position in the apo structure. Pro236, which is located on the intervening turn, translates approximately 3 Å.[14] This movement allows for the formation of a direct hydrogen bond between the carbonyl of Pro236 and the Lys103 amide NH and provides favorable hydrophobic interactions between the aniline portion of the inhibitors and hydrophobic elements of the underlying shifted β sheet (Figure 1b).

Another class of NNRTIs contains a hydrogen bond acceptor that directly interacts with the Lys103 backbone NH. In addition to delavirdine, this group includes many "next-generation" inhibitors that maintain potency against the commonly observed Lys103Asn mutant virus.[4,6] Structural analysis of these compounds bound to HIV-RT shows that the β13−β14 turn region is in a position similar to that found in the unliganded structure (Figure 1c). The inhibitors that interact with the backbone of Lys103 fill the space adjacent to the loop with functionality capable of maintaining substantial hydrophobic contacts with P236 and F227. For example, the investigational drug candidates **31** (GW678248)[17] and **32** (RDEA806)[18] contain an aromatic
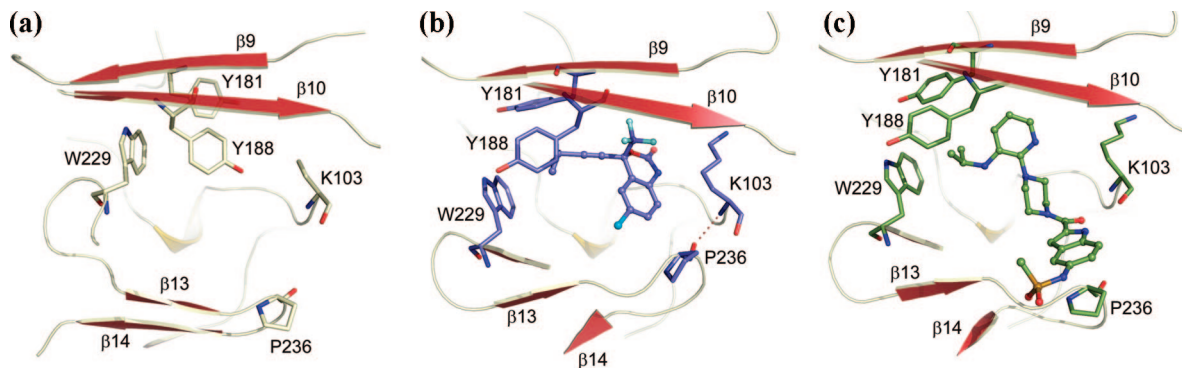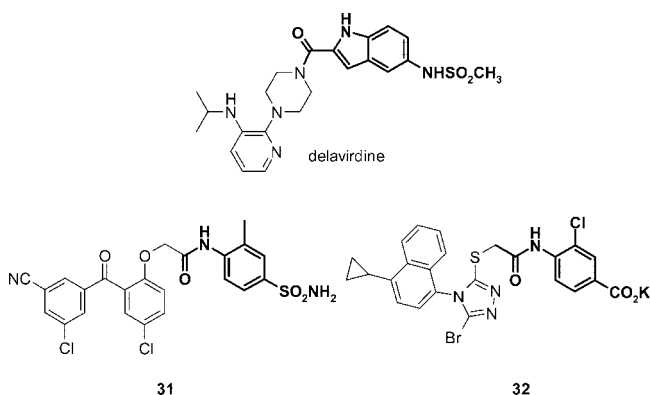
Figure 1. (a) NNRTI binding pocket in apo enzyme structure (1HMV). (b) Structure of efavirenz in the NNRTI binding pocket (1FK9). Reorganization of the protein creates volume to accommodate the NNRTI. Smaller compounds such as this one result in an inward motion of P236 that hydrogen-bonds to the backbone of K103. (c) Structure of delavirdine in NNRTI binding pocket (1KLM). The larger compound stabilizes Pro236 and the flanking β strands in a more open conformation.

Chart 2. NNRTIs Delavirdine, **31**, and **32**, Highlighting the Portions of the Inhibitor That Contact Lys103 and Pro236

Scheme 1. Preparation of Ester Intermediates **15**[a]

[a] (a) NaO-*t*-Bu, 2,3,4-trifluoronitrobenzene, THF, 0 °C; (b) (i) NaH, *tert*-butyl ethylmalonate, NMP; (ii) **12**, NMP, 0 °C to room temperature; (c) TFA, dichloroethane, 75 °C (d) (i) Fe, NH$_4$Cl, EtOH, H$_2$O, 80 °C; (ii) NaNO$_2$, aqueous hydrogen bromide, CuBr, LiBr, CH$_3$CN, 30 °C; (e) LiOH, CH$_3$CN, H$_2$O, room temperature; (f) (BOC)$_2$O, DMAP, *t*-BuOH, EtOAc, 40 °C.

amide functionality in which the amide portion of the inhibitor interacts with the Lys103 NH while the substituted phenyl group makes extensive hydrophobic contacts (Chart 2).

In earlier studies of diaryl ether NNRTIs, we had discovered that triazolinones related to structure **A** are potent inhibitors of viral replication (Figure 2).[19] Structural analysis revealed that the triazolinone ring simultaneously forms hydrogen bonds with the carbonyl and amide NH functionality of Lys103. Modeling of the triazolinones **A** and similar amide-based inhibitors **B** indicated that the amides made more extensive contact with the β13–β14 region. This observation led to the design of annulated pyrazole NNRTIs **C**, which should make hydrogen bonding interactions similar to those of the triazolinone while more effectively engaging in hydrophobic interactions with the distal portions of the β12–β14 sheet. In this paper, we describe the
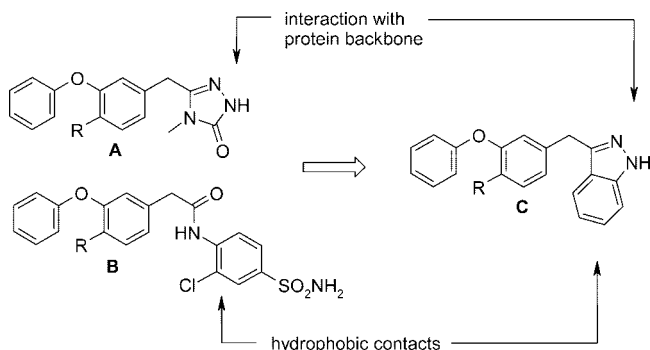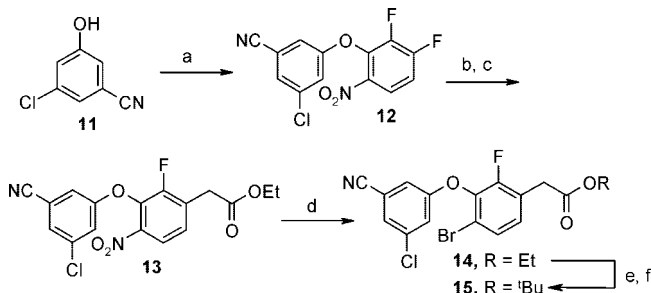
discovery of annulated pyrazole NNRTIs that maintain excellent activity against wild-type and NNRTI-resistant viruses.[20] Structural analysis reveals a distribution of significant interactions between the most potent inhibitors and HIV-RT. These contacts allow this class of compounds to inhibit a broad range of NNRTI-resistant viruses.

Chemistry

The synthesis of the diaryl ether NNRTIs commenced with a highly regioselective reaction between phenol and 2,3,4-trifluoronitrobenzene as described in Scheme 1. A malonate addition/decarboxylation sequence allowed for the installation of the acetic acid ester group in good yield. Reduction of the nitro functionality and a Sandmeyer reaction with the resulting aniline gave ester **14**. The ethyl ester could be converted to the corresponding *tert*-butyl ester **15** using standard procedures.

The synthetic procedure used for the preparation of annulated pyrazole NNRTIs starting from **14** is exemplified for compound **4** in Scheme 2. In the key transformation, a Claisen condensation between an acylimidazole and the sodium enolate of ester **14** or **15** provided β-ketoesters that could be decarboxylated and treated with hydrazine to provide the annulated pyrazole inhibitors. This route proved to be generally useful for the preparation of pyrazoles that contained different functionality on the annulated phenyl ring. The acid utilized for the preparation of pyrazolo[3,4-*c*]pyridazines **6** and **8**–**10** was prepared in four steps starting from commercially available 3-carboxy-2,6-dichloropyridazine (Scheme 3). Similarly, pyrazolopyridone **3** was prepared employing acid **24** (synthesis

Figure 2. Design of annulated pyrazole NNRTIs.

Scheme 2. General Synthesis of Annulated Pyrazole Analogues[a]
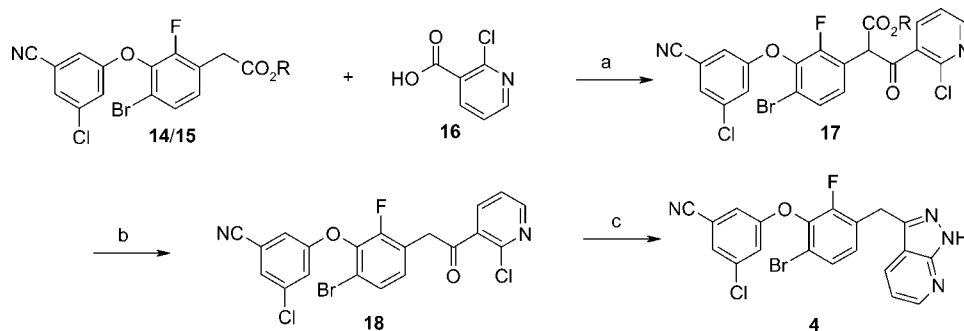
[a] (a) **16**, 1,1'-carbonyldiimidazole, DMF, 50 °C; then **14** or **15**, NaH, −10 °C.; (b) for R = Et, H₂O, DMSO, 150 °C; for R = *t*-Bu, TFA, CH₂Cl₂, room temperature; (c) hydrazine, EtOH, 50 °C.

Scheme 3. Preparation of Pyridazine Acid for the Synthesis of Inhibitors **6** and **8−10**[a]
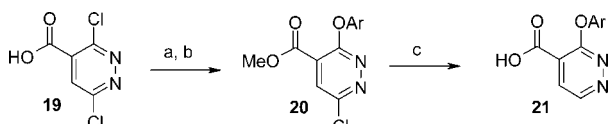
[a] (a) Trimethylsilyldiazomethane, MeOH, CH₂Cl₂, 0 °C; (b) 2,4-difluorophenol, NaH, THF, 0−50 °C; (c) palladium on carbon, ammonium formate, MeOH, room temperature to 60 °C; then LiOH, THF, MeOH, H₂O, room temperature.

Scheme 4. Preparation of Pyridone Acid **24**[a]
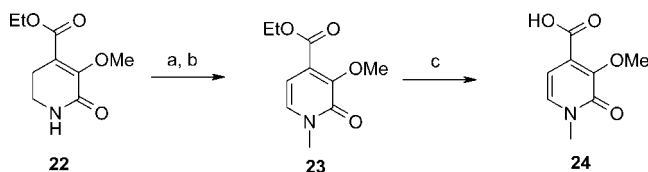
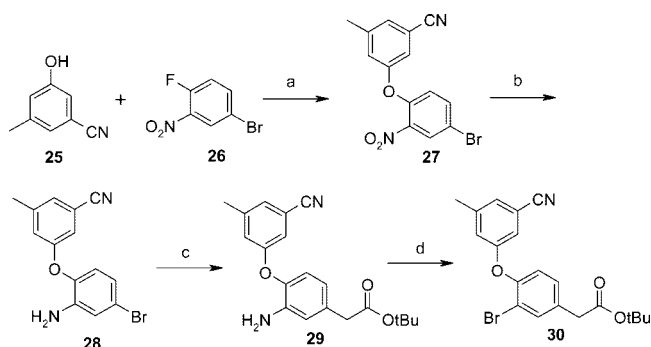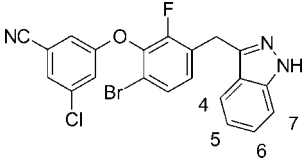[a] (a) Pd carbon, xylenes, 160 °C; (b) CH₃I, K₂CO₃, DMF, 50 °C; (c) LiOH, THF, room temperature.

Scheme 5. Synthesis of Ester Intermediate **30**[a]

[a] (a) K₂CO₃, DMF, room temperature; (b) Fe, NH₄Cl, H₂O, EtOH, 100 °C; (c) 2-*tert*-butoxyethylzinc chloride, bis(tri-*tert*-butylphosphine)palladium, dioxane, room temperature; (d) *t*-BuONO, CuBr₂, LiBr, CH₃CN, 60 °C.

Table 1. Structure and Activity of Annulated Pyrazole Compounds **1−7**

compd	X₇	X₆	X₅	X₄	IC₅₀, nM[a]		EC₅₀, nM[b]	
					WT	103N/181C	WT	103N/181C
1	CCN	CH	CH	CH	24	15	5	53
2	CNH₂	CH	CH	CH	24	22	8	84
3	C=O	NCH₃	CH	CH	8	12	4	97
4	N	CH	CH	CH	8	nt[c]	1	12
5	CH	N	CH	CH	5	9	2	18
6	N	N	CH	CH	3	3	1	4
7	N	CH	CH	N	3	14	25<	>100

[a] Inhibition of RNA-dependent DNA polymerase activity using the wild type or Lys103Asp/Tyr181Cys polymerase. [b] Inhibition of virus-induced cell death in MT-4 cells. [c] Not tested.

Results and Discussion

The inhibitors **1−7** were evaluated in enzymatic and cellular assays using standard procedures, and the results are displayed in Table 1. Inhibition of HIV polymerase activity was initially assessed using purified recombinant wild-type or Lys103NAsn/Tyr181Cys HIV polymerase and a poly(rA)/oligo(dT)₁₆ template-primer. The ability of the NNRTIs to reduce HIV replication in cell culture was determined in MT-4 cells using wild-type virus and clinically relevant mutant strains. Further details are provided in the Experimental Section.

In order to test the hypothesis that annulated pyrazole compounds would be potent inhibitors of polymerase activity, compound **1** was initially prepared (Table 1). Modeling had suggested that the nitrile substituent of the indazole ring would emerge from the binding pocket through an opening that separates Lys104 and Pro225, and we were encouraged to find that this compound did exhibit strong inhibition of polymerase activity in the enzyme assay. Furthermore, **1** displayed good potency in the cellular antiviral assay. Replacement of the nitrile of the indazole ring with an amino group (**2**) or conversion of the indazole phenyl ring to a methylated pyridone (**3**) did not significantly alter activity against the wild-type or mutant viruses. Pyrazolopyridine **4**, which contains a single nitrogen atom in the 7-position of the phenyl ring, had excellent activity in the cellular assay. This potency was maintained for regioisomer **5**. Additional activity was gained for the pyrazolo[3,4-c]pyridazine **6**, which significantly inhibited virus replication at subnanomolar concentrations in the cellular assay. Isomeric

described in Scheme 4). The ester intermediate used for the synthesis of compound **10** was prepared in four steps as described in Scheme 5. A nucleophilic aromatic substitution reaction between phenol **25** and fluorobenzene **26** provided the diaryl ether. Acetic acid ester **29** was prepared by reduction of the nitro group with iron, followed by a palladium-catalyzed reaction with 2-*tert*-butoxyethylzinc chloride. A Sandmeyer reaction was then used to install the desired halogen.

Chart 3. Additional Pyrazolo[3,4-c]pyridazine Inhibitors

8

EC$_{50}$ (wt): 1 nM
EC$_{50}$ (103N/181C): 5 nM

9

EC$_{50}$ (wt): 1 nM
EC$_{50}$ (103N/181C): 3 nM

10

EC$_{50}$ (wt): 17 nM
EC$_{50}$ (103N/181C): >100 nM
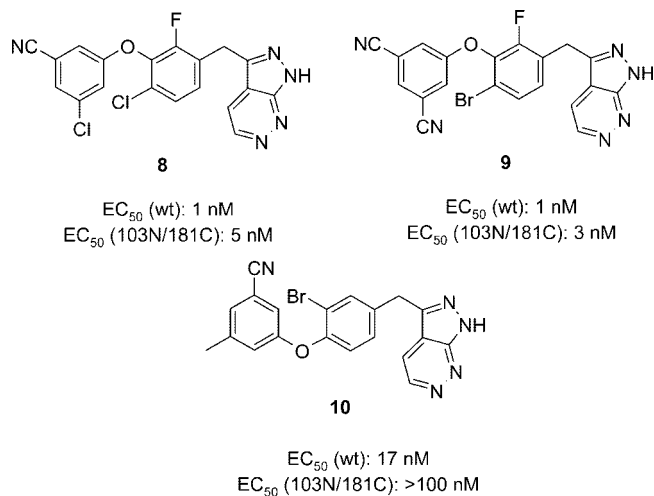
compounds in which the nitrogen atom in the 6-position was moved to other positions (e.g., **7**) generally had inferior potency in the cellular assay, particularly in tests with the Lys103Asn/Tyr181Cys mutant enzyme.

The pyrazolopyridazine heterocycle found in inhibitor **6** was used to prepare a small family of NNRTIs (Chart 3). Compounds **8** and **9** were also found to maintain good potency against the wild-type and mutant viruses. Inhibitor **10**, which was prepared in order to test the requirement for a meta disposition of the methylene and ether linkages about the central phenyl ring, had reasonable activity against the wild-type virus but did not inhibit the Lys103Asn/Tyr181Cys mutant at tested concentrations. Further investigation revealed that **10** also did not maintain good potency against the Lys103Asn or Tyr181Cys single mutant viruses (IC$_{50}$(wt) = 30 nM, IC$_{50}$(Lys103Asn) = 120 nM, IC$_{50}$(Tyr181Cys) = 800 nM).

Compound **8**, which had an excellent preliminary antiviral profile and moderate molecular weight (MW = 415 Da), was selected for further profiling. Tests with a large panel of NNRTI-resistant mutant viruses revealed that single nucleotide mutations of the wild-type virus do not significantly reduce the potency of this compound (Table 2). In particular, **8** strongly inhibits replication of the prevalent 103Asn, 181Cys, and 190Ala mutants. For comparison, data obtained with efavirenz are also shown. Inhibitor **8** was more potent than efavirenz against several NNRTI resistant mutants and the wild-type virus. The relative potencies of efavirenz and **8** in this assay against the Lys103Asn mutant were particularly striking.

The potential of compound **8** to prevent the replication of NNRTI-resistant viruses that contain several mutations of the viral genome was assessed in testing against a panel of NNRTI-resistant clinical isolates (Table 3). These viruses were selected (PhenoScreen, Monogram Biosciences) on the basis of their reduced susceptibility to efavirenz, and the diversity of viral isolates was chosen to represent the majority of NNRTI resistance patterns that have been described in clinical practice. Etravirine, which has shown excellent potency against NNRTI-resistant viruses,[15] was also tested for its ability to inhibit the

replication of the isolates. Compound **8** and etravirine were able to effectively inhibit a similar proportion of viruses in this panel (effective inhibition defined as (IC$_{50}$ mutant)/(IC$_{50}$ wild-type) < 10). Importantly, compound **8** maintained potency against all viruses that contained the common K103 and Y181 mutations. A substantial (>10-fold) reduction in potency was observed only for isolates that contain the Y188L/G190A and A98/V108/G190/F227 combination mutations.

Pharmacokinetic profiling revealed that **8** is also stable in vivo (Table 4). This inhibitor had a moderate volume of distribution, and acceptable half-lives were observed in several preclinical species.

The structures of compounds **6** and **10** bound to wild-type HIV-RT were solved in order to further understand the binding mode of the inhibitors to HIV-RT (Figures 3 and 4). As designed, the compounds induce the expanded NNRTI pocket where Pro236 and the flanking ends of strands β13 and β14 are in a position similar to that found in the apo structure. This configuration is stabilized by the pyrazolopyridazine moiety. The pyrazole makes hydrogen bonds to both the backbone amide and carbonyl of Lys103. The pyridazine extension parallels the face of Pro236 of the β13−β14 hairpin, and its amphipathic edges are well suited to the site: the hydrophobic edge faces the pocket interior, packing with Phe227 and Leu234, while the polar nitrogen atoms of the six-membered ring are exposed to solvent through one of the few openings of the highly buried cavity (Figure 5).

The diaryl ether system of both **6** and **10** partly overlaps the "butterfly wing" binding region of the early NNRTIs,[21] but the two inhibitors maintain markedly different angles through the ether linkage. Both **6** and **10** sit closer to strands β6 and β10 than most NNRTIs, which allows Tyr181 to remain in the general position it occupies in apo or DNA-bound RT structures.[22,23] Concomitantly, Tyr188 rotates slightly to form aromatic stacking interactions with the terminal phenyl ring of the inhibitors. This portion of the molecule is also braced against the conserved Trp229 residue, and a distortion of strand β12 and the primer grip region similar to that observed in first-generation NNRTIs is achieved. The large bromine on the core ring of **6** fills the volume between Val106, Val179, Tyr181, and Tyr188, with closest approach (3.5 Å) to the backbone carbonyl of Tyr188, suggesting a favorable halogen−carbonyl interaction as seen in other recent examples.[24]

The primary difference between compounds **6** and **10** is the relative disposition of the substituents about the central phenyl ring (Figure 6). Compound **10** also extends more broadly across the binding pocket, reaching slightly closer to both Trp229 at the back of the pocket and Lys103 at the opposite side. While the amino acids on each end of the pocket shift outward slightly to accommodate the ligand, the tightness of fit and the lower potency of **10** compared to **6** suggests that the organization of the inhibitor may extend beyond the optimal size for the wild type pocket. The central phenyl ring of **10** is pivoted such that the bromine atom does not interact significantly with the Tyr188 carbonyl group and has fewer contacts in this hydrophobic subpocket. The central phenyl ring of **10** is also removed from the carbonyl group of K101 relative to the more potent inhibitor

Table 2. Potency of **8** and Efavirenz against WT-HIV and Selected NNRTI-Resistant Mutant Viruses[a]

compd	WT	WT[b] 40%	190A	190S	100 I	101E	225H	103N	106A	108I	179D	227 L	236 L	138K	181I	188H	181C
8	1	5	1	<1	<1	2	<1	<1	2	1	1	1	1	2	1	<1	1
EFV	2	18	6	>100	7	12	1	66	6	3	8	1	<1	2	2	4	3

[a] EC$_{50}$ (nM) for inhibition of virus-induced cell death in MT-4 cells. [b] Tests performed in the presence of 40% human serum.

Table 3. IC$_{50}$ for **8** and Etravirine against NNRTI-Resistant Clinical Isolates[a]

virus	**8**	Etr	NNRTI-associated mutations
CNDO	1	2	
1	100	2	G190, Y188
2	10	28	A98, K101, Y181, G190
6	2	6	L100, K103
12	1	6	L100, K103
14	3	1	A98, K103, V108, M230
16	3	1	K103, P225
17	5	14	A98, K103, Y181
20	4	7	K103, Y181
21	3	17	K103, V179, Y181
29	2	3	K103, Y181
31	7	73	A98, V179, Y181
32	7	9	V106, V179, Y181, G190
34	5	5	K101, V106, Y181
36	2	3	K103, V106, Y181
43	6	13	K103, Y181, P225
47	24	1	A98, V108, G190, F227

[a] IC$_{50}$ (nM) in Monogram Biosciences PhenoScreen single-cycle antiviral assay. Etr = etravirine.

**Table 4.** Selected Pharmacokinetic Parameters for Compound **8**[a]

species	Cl ((mL/min)/kg)	V_{ss} (L/kg)	$T_{1/2}$ (h)
rat	2.9	0.91	4.2
dog	4.6	0.99	5.6
monkey	1.3	1.21	12.2

[a] Clearance, volume, and half-life observed following intravenous administration of 0.5 mg/kg dose in 30% DMSO/55% PEG-400/15% water.
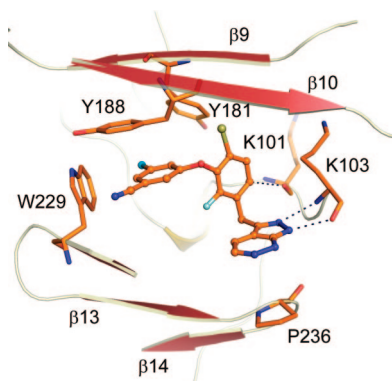
Figure 3. Structure of compound **6** in the NNRTI binding pocket (3DYA). The diaryl ether fills the core hydrophobic pocket. The pyrazolo[3,4-c]pyridazine forms hydrogen bonds to the backbone of K103 and stabilizes Pro236 in an apo-like position, creating an expanded pocket volume relative to efavirenz.

6. Many NNRTIs maintain a strong hydrogen bond donor–acceptor relationship with the carbonyl group of Lys101, and it is possible that the CH–hydrogen bond through which **6** interacts with this moiety contributes to the activity of the inhibitor (Figure 3).[25]

As has been noted previously, NNRTI-resistant HIV-reverse transcriptases generally have an expanded pocket volume relative to the wild type enzyme.[12] That is, the majority of NNRTI resistance-pathways involve the substitution of residues that make hydrophobic interactions with the enzyme inhibitor. As a consequence of the larger size of compound **6** and the expanded binding pocket that it induces in the reverse transcriptase enzyme, the interactions of this inhibitor are spread across a larger area of the protein than first generation NNRTIs. All portions of the molecule are making significant interactions with the enzyme, and no individual position appears to provide a majority of the interaction energy. This conclusion is supported by the observation that perturbation of the significant interactions
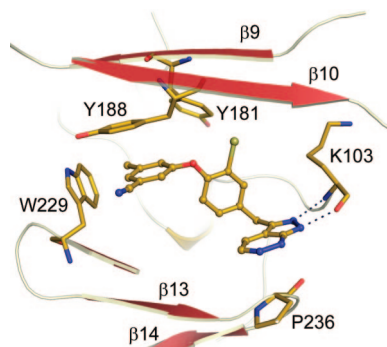
Figure 4. Structure of compound **10** in the NNRTI binding pocket (3E01). The pocket is formed similarly to compound **6**, though the para disposition around the core forces slight setbacks of W229 and K103.
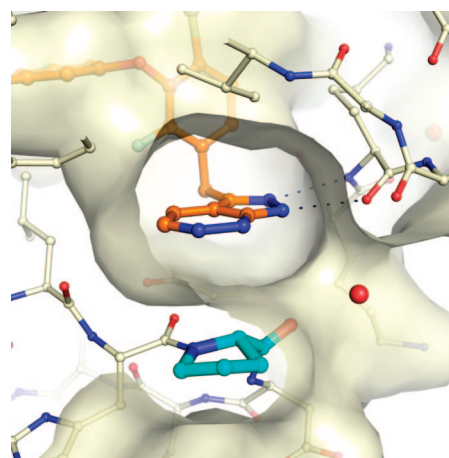
Figure 5. View of the pyrazolo[3,4-c]pyridazine ring in the **6**–RT complex. On the pyrazole moiety, the carbon atoms face the interior hydrophobic environment while the nitrogen atoms are relatively exposed to solvent via a small opening in the enclosed binding pocket.

between the pyrazolopyridazine compounds and mutable residues such as Val106, Tyr188, and Phe227 does not significantly impact the inhibition potency. In addition, the architecture of **6** includes malleable linkages that allow for conformational and positional adjustment.[26–28] As a consequence of the soft energy potentials around those connections, binding energy is lost as the compound adapts to the mutant protein's changed surface. Finally, specific polar interactions target invariant backbone atoms rather than mutable side chain groups. These motifs are again spread across the binding pocket and include traditional hydrogen bond interactions with the pyrazolopyridazine heterocycle, CH–hydrogen bond interactions of the central phenyl ring, and halogen–carbonyl interactions of the bromine atom. Some of these interactions are not observed in the structure of the enzyme complex with inhibitor **10**, and their absence may contribute to the relatively poor potency of this inhibitor.

Conclusions

Structure-based design of novel inhibitors that interact with the K103 backbone of HIV-reverse transcriptase has led to the discovery of NNRTIs that contain an unusual 1H-pyrazolo[3,4-c]pyridazine heterocycle. This heterocycle stabilizes a large binding pocket with many structural features less changed from the apoprotein conformation than seen in early NNRTIs. The optimized fit to this expanded pocket provides compounds that potently inhibit the replication of wild-type and NNRTI-resistant
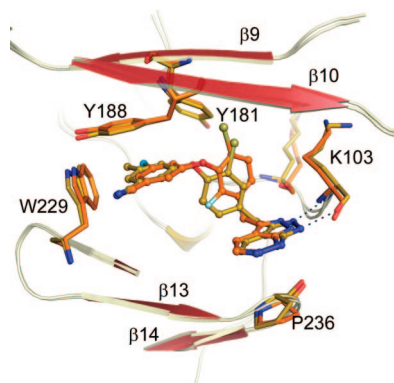
Hz, 1H), 7.06 (m, 1H), 4.21 (q, $J = 7.1$ Hz, 2H), 3.80 (d, $J = 1.5$ Hz, 2H), 1.28 (t, $J = 7.1$ Hz, 3H).

[4-Bromo-3-(3-chloro-5-cyanophenoxy)-2-fluorophenyl]acetic Acid Ethyl Ester (14). A 250 mL round-bottom flask was charged with **13** (8.0 g, 21.12 mmol) and absolute EtOH. To the reaction vessel was added NH$_4$Cl (2.26 g, 42.2 mmol), water (30 mL), and iron (1.17 g, 21.1 mmol). The mixture was stirred and heated to 80 °C for 4 h. When **13** was consumed, the heterogeneous mixture was filtered and the filter cake was washed with EtOAc. The aqueous filtrate was extracted with EtOAc and washed with water and brine. The combined EtOAc extracts were dried over Na$_2$SO$_4$ and filtered. The solvent was removed in vacuo to afford a pale oil which was purified by column chromatography, eluting with EtOAc/hexane (15:85) to afford the aniline (6.0 g, 87%). The aniline (20.0 g, 57.3 mmol), CuBr (24.7 g, 172 mmol), and LiBr (7.45 g, 86.0 mmol) were placed in CH$_3$CN (400 mL) and heated to 30 °C. A 48% aqueous HBr solution (13.0 mL, 115 mmol) was added, which resulted in a slight exotherm. Sodium nitrite (11.5 mL of a 40% aqueous solution, 86 mmol) was slowly added over 30 min, during which time the starting material was consumed and the solution became homogeneous. The solution was stirred for an additional hour, solid NaHSO$_3$ (6.0 g) and SiO$_2$ (40 g) were added, and the mixture was cooled to room temperature. The acetonitrile solvent was removed by distillation, toluene (400 mL) was added, and the solution was filtered. The toluene was removed by distillation, and the remaining solids were crystallized from isopropyl alcohol and water to provide **14** (20.2 g, 85%). ^{1}H NMR (DMSO-d_6): δ 7.82 (t, $J = 1.5$ Hz, 1H), 7.51−7.47 (m, 2H), 7.43−7.40 (m, 2H), 4.11 (q, $J = 7.1$ Hz, 2H), 3.84 (s, 2H), 1.29 (t, $J = 7.1$ Hz, 3H).

[4-Bromo-3-(3-chloro-5-cyanophenoxy)-2-fluorophenyl]acetic Acid *tert*-Butyl Ester (15). A solution of **14** (15 g, 0.036 mol) in acetonitrile (75 mL) was heated to 50 °C. An aqueous solution of lithium hydroxide (1.6 g in 10 mL water, 1.1 equiv) was added over 2.5 h with stirring. The mixture was stirred overnight at 50 °C, diluted with toluene (100 mL), and cooled to 5 °C. After aging the mixture for 1 h at 5 °C, the mixture was filtered, washed with cold acetonitrile, and dried in a vacuum oven to provide the lithium salt of [4-bromo-3-(3-chloro-5-cyanophenoxy)-2-fluorophenyl]acetic acid (12.9 g, 92%). This salt was suspended in MTBE (20 mL/g) and washed three times with 10% sulfuric acid in water. The organic layer was washed with brine, decolorizing carbon (75 mg/g, Darco KB) and silica gel (75 mg per gram) were added, and the mixture was stirred at ambient temperature for 2 h. The mixture was filtered and concentrated under reduced pressure to provide the acid as an oil that solidified on standing. The acid (12.7 g, 0.033 mol, 1 equiv), *tert*-BuOH (2.45 g, 5 equiv), Boc$_2$O (7.20 g, 1.05 equiv), and DMAP (120 mg, 0.03 equiv) were dissolved in EtOAc (33 mL). The mixture was warmed to 40 °C for 3 h and cooled to room temperature, and an equal volume of water was added, followed by H$_2$SO$_4$ (4 equiv). The aqueous layer was separated and discarded, and the organic layer was washed with water. The organic layer was washed with brine, concentrated to about 20% of original volume, and diluted with hexanes back to the original volume. Decolorizing carbon (75 mg/g, Darco G60) and silica gel (75 mg/g) were added, and the mixture stirred at ambient temperature for 2 h. The mixture was filtered and concentrated under reduced pressure to give the ester as an oil that solidified on standing (12.4 g, 85%). ^{1}H NMR (CDCl$_3$): δ 7.44 (m, 1H), 7.34 (m, 1H), 7.15 (m, 2H), 7.04 (m, 1H), 3.61 (s, 1H), 1.44 (s, 9H).

General Procedure for Preparation of 1−10 from Ester 14. Step 1. Synthesis of 3-(6-Bromo-3-{2-[2-(2,4-difluorophenoxy)pyridin-3-yl]-2-oxoethyl}-2-fluorophenoxy)-5-chlorobenzonitrile (18). CDI (1.57 g, 9.7 mmol) was added to a solution of acid **17** (1.45 g, 9.2 mmol) in dry DMF (30 mL). The solution was heated to 50 °C for 1 h and then cooled to −10 °C. A solution of ester **14** (4.00 g, 9.7 mmol) in DMF (15 mL) was added, followed by a 60% dispersion of NaH (1.35 g, 31 mmol). The orange solution was warmed slowly to room temperature, stirred for 30 min, and added to a saturated aqueous solution of ammonium chloride. The aqueous layer was extracted with EtOAc. The combined organic layers were washed with brine, dried over MgSO$_4$, filtered, and concentrated

Figure 6. Compound **6** (3DYA) and compound **10** (3EO1) in the NNRTI binding pocket.

viruses. Pharmacokinetic studies revealed that inhibitor **8** has properties suitable for use as an NNRTI that could provide improved treatment durability for HIV-infected patients. These compounds and related diaryl ether NNRTIs will be the subject of future reports.

Experimental Section

NMR spectra were recorded on a Bruker 300 MHz or Bruker 400 MHz spectrometer. Elemental analyses were performed at Roche Palo Alto. All purchased starting materials were used without further purification. Solvents used in reaction mixtures were anhydrous and stored under nitrogen. All reactions were performed in oven-dried flasks under a nitrogen atmosphere unless otherwise noted.

3-Chloro-5-(2,3-difluoro-6-nitrophenoxy)benzonitrile (12). A 250 mL round-bottom flask was charged with (6.0 g, 39.0 mmol) and anhydrous THF (100 mL), and the solution was cooled to 0 °C. To the cooled solution was added sodium *tert*-butoxide (46.9 g, 45.0 mmol), and the resulting solution stirred for 1 h. 2,3,4-Trifluoronitrobenzene (6.9 g, 39.0 mmol) was added dropwise while maintaining the mixture at 0 °C until the phenol was completely consumed. The mixture was quenched by addition of 10% aqueous HCl, and the resulting mixture was stirred for an additional hour. The mixture was extracted with EtOAc and washed with water and brine. The EtOAc was dried over Na$_2$SO$_4$ and filtered. The solvent was removed in vacuo to yield a yellow oil which was purified by column chromatography on silica gel with EtOAc/hexanes to afford ether **12** (10 g, 82%). ^{1}H NMR (DMSO-d_6): δ 8.20 (m, 1H), 7.85 (m, 1H), 7.75−7.70 (m, 3H).

[3-(3-Chloro-5-cyanophenoxy)-2-fluoro-4-nitrophenyl]acetic Acid Ethyl Ester (13). A solution of *tert*-butyl ethyl malonate (10.3 g, 54.8 mmol) in anhydrous NMP (200 mL) was cooled to 0 °C and stirred under a nitrogen atmosphere. To this solution was added NaH (40% in mineral oil, 1.84 g, 76.7 mmol). The mixture was allowed to stir at 0 °C for 1 h. The aryl ether **12** (15.00 g, 49.80 mmol) was then added to the reaction vessel and stirred under nitrogen at room temperature until the reaction was complete. The mixture was quenched by addition of aqueous 10% HCl at room temperature, extracted with EtOAc, and washed with water and brine. The EtOAc was dried over Na$_2$SO$_4$ and filtered, and the solvent was removed in vacuo to afford a light-yellow oil. This oil (24.0 g, 50.2 mmol) was dissolved in dichloroethane (300 mL) and TFA (6.29 g, 55.2 mmol) and heated to 75 °C for 24 h. The mixture was cooled to room temperature, and solvent and excess TFA were removed in vacuo. The crude oil was dissolved in CH$_2$Cl$_2$ and cooled to 0 °C, and aqueous NaHCO$_3$ was added. The mixture was extracted with CH$_2$Cl$_2$ and washed with water and brine. The organic layer was dried over Na$_2$SO$_4$ and filtered, and the solvent was removed in vacuo to afford a yellow oil. The crude oil was purified by column chromatography on silica gel, eluting with EtOAc/hexanes (1:9) to afford **13** (15.0 g, 80%). ^{1}H NMR (CDCl$_3$): δ 7.89 (dd, $J = 8.5$ Hz, 1.9 Hz, 1H), 7.41 (m, 2H), 7.20 (t, $J = 2.2$

in vacuo to provide an orange oil. This oil was dissolved in DMSO (20 mL) and brine (1 mL), and the solution was placed in a oil bath that had been heated to 150 °C. After 10 min, the mixture was poured into water (500 mL) and the aqueous mixture was extracted with EtOAc. The combined organic layers were washed with brine, dried over $MgSO_4$, filtered, and concentrated. The residue was purified by column chromatography on silica gel, eluting with a EtOAc/hexanes gradient (25−100% EtOAc) to provide 18 (3.32 g, 73%) as a white solid. ^{1}H NMR ($CDCl_3$): δ 8.54 (dd, J = 4.7 Hz, 1.5 Hz, 1H), 7.88 (dd, J = 8.2 Hz, 1.6 Hz, 1H), 7.49 (dd, J = 8.2 Hz, 1.8 Hz, 1H), 7.37 (m, 2H), 7.16 (m, 2H), 6.99 (m, 1H), 4.39 (s, 1H).

Step 2: 3-[6-Bromo-2-fluoro-3-(1H-pyrazolo[3,4-b]pyridin-3-ylmethyl)phenoxy]-5-chlorobenzonitrile (4). Hydrazine (0.44 mL, 2 equiv) was added to a solution of the ketone 18 (3.32 g, 6.9 mmol) in a mixture of dioxane (20 mL) and EtOH (3 mL), and the solution was slowly heated to 50 °C. After 2 h, the volatile materials were removed, and the solid was triturated with a 1:1 mixture of EtOAc and hexanes. The remaining solids were dissolved in 25% MeOH/CH_2Cl_2 and washed with water, saturated aqueous $NaHCO_3$ solution, and brine. The volatile materials were removed in vacuo to provide the desired product 4 (1.90 g, 59%). ^{1}H NMR (DMSO-d_6): δ 13.43 (s, 1H), 8.50 (dd, J = 4.5 Hz, 1.5 Hz, 1H), 8.10 (dd, J = 8.0 Hz, 1.6 Hz, 1H), 7.80 (m, 1H), 7.59 (dd, J = 8.4 Hz, 1.8 Hz, 1H), 7.48 (dd, J = 2.4 Hz, 1.3 Hz, 1H), 7.40 (t, J = 2.2 Hz, 1H), 7.26 (m, 1H), 7.15 (dd, J = 8.1 Hz, 4.5 Hz, 1H), 4.37 (s, 2H). MS (ESI): 457 (M + H). Anal. Calcd for $C_{20}H_{11}BrClFN_4O\cdot0.4H_2O$: C, 51.67; H, 2.56; N, 12.05. Found: C, 51.67; H, 2.55; N, 12.42.

3-[4-Bromo-3-(3-chloro-5-cyanophenoxy)-2-fluorobenzyl]-1H-indazole-7-carbonitrile (1). 1 was prepared as described in the general procedure from 3-cyano-2-fluorophenylacetic acid and 14 (24% overall yield). ^{1}H NMR (DMSO-d_6): δ 13.81 (s, 1H, NH), 8.06 (d, J = 8.3 Hz, 1H), 7.93 (d, J = 8.3 Hz, 1H), 7.80 (m, 1H), 7.58 (dd, J = 8.3 Hz, 1.7 Hz, 1H), 7.48 (dd, J = 2.5, 1.2 Hz, 1H), 7.40 (t, J = 2.1 Hz, 1H), 7.25 (m, 2H), 4.41 (s, 1H). MS (ESI): 484 (M + H). Anal. Calcd for $C_{22}H_{11}BrClFN_4O\cdot0.25H_2O$: C, 54.34; H, 2.38; N: 11.53. Found: C, 54.71; H, 2.31; N, 11.18.

3-[3-(7-Amino-1H-indazol-3-ylmethyl)-6-bromo-2-fluorophenoxy]-5-chlorobenzonitrile (2). As described in the general procedure, 3-[6-bromo-2-fluoro-3-(7-nitro-1H-indazol-3-ylmethyl)phenoxy]-5-chlorobenzonitrile was prepared in 15% overall yield from 2-chloro-3-nitrobenzoic acid and 14. This material (0.070 g, 0.013 mmol) was dissolved in EtOH (0.4 mL) and H_2O (0.1 mL). Iron powder (0.032 g, 0.058 mmol) and NH_4Cl (0.031, 0.058 mmol) were added. The solution was heated to 90 °C for 30 min, cooled to room temperature, filtered, and concentrated in vacuo to provide the amine. The resulting product was purified by column chromatography on silica gel, eluting with an EtOAc/hexane gradient (33−70% EtOAc) to afford 2 (0.068 g, 91%). ^{1}H NMR (DMSO-d_6): δ 12.36 (s, 1H, NH), 7.80 (m, 1H), 7.54 (dd, J = 8.5, 1.7 Hz, 1H), 7.47 (dd, J = 2.3, 1.2 Hz, 1H), 7.39 (t, J = 2.2 Hz, 1H), 7.2 (m, 1H), 6.77 (m, 2H), 6.45 (dd, J = 6.7 Hz, 1.4 Hz, 1H), 5.28 (s, 2H, NH_2), 4.26 (s, 2H). MS (ESI): 471 (M + H). Anal. Calcd for $C_{21}H_{13}BrClFN_4O$: C, 53.47; H, 2.78; N, 11.88. Found: 53.51; H, 2.63; N, 11.65.

3-Methoxy-1-methyl-2-oxo-1,2-dihydropyridine-4-carboxylic Acid Ethyl Ester (23). Palladium on carbon (1.2 g of a 10 weight-percent dispersion) was added to ester 22 (5.30 g, 28.6 mmol) that was suspended in xylenes (100 mL). This mixture was then heated to 160 °C for 20 h. Upon cooling, the mixture was diluted with 1:1 MeOH/$CHCl_3$ (200 mL) and filtered. The solution obtained was concentrated in vacuo. This material was redissolved in DMF (100 mL), and to the mixture was added K_2CO_3 (20.3 g, 143 mmol) and iodomethane (7.2 mL, 114 mmol). After being stirred for 3 h at 50 °C, the mixture was filtered, quenched with 10% HCl (30 mL), diluted with water, and extracted with EtOAc. The organic layers were washed with brine, dried over $MgSO_4$, filtered, and concentrated. Column chromatography on silica gel, eluting with a EtOAc/hexanes gradient (50−100% EtOAc), provided the ethyl ester 23 (2.14 g, 35%). ^{1}H NMR ($CDCl_3$): δ 7.07 (d, J = 7.3 Hz, 1H),

6.33 (d, J = 7.3 Hz, 1H), 4.36 (q, J = 7.1 Hz, 2H), 4.01 (s, 3H), 3.57 (s, 3H), 1.38 (t, J = 7.1 Hz, 3H).

3-Methoxy-1-methyl-2-oxo-1,2-dihydropyridine-4-carboxylic Acid (24). Ethyl ester 23 (0.75 g, 3.6 mmol) was dissolved in THF (35 mL). To this solution was added a solution of $LiOH\cdot H_2O$ (0.18 g, 4.2 mmol) in H_2O (12 mL). After being stirred for 18 h, the mixture was quenched with 10% HCl to pH 1 and extracted with EtOAc. The organic layers were washed with brine, dried over $MgSO_4$, filtered, and concentrated to provide acid 24 (0.55 g, 85%). ^{1}H NMR ($CDCl_3$): δ 7.17 (d, J = 7.1 Hz, 1H), 6.73 (d, J = 7.1 Hz, 1H), 4.28 (s, 3H), 3.60 (s, 3H).

3-[6-Bromo-2-fluoro-3-(6-methyl-7-oxo-6,7-dihydro-1H-pyrazolo[3,4-c]pyridin-3-ylmethyl)phenoxy]-5-chlorobenzonitrile (3). 1,1′-Carbonyldiimidazole (0.53 g, 3.6 mmol) was added in one portion to a solution of acid 24 (0.55 g, 3.25 mmol) in DMF (5.0 mL). After being heated for 30 min at 50 °C, the solution was cooled to 0 °C and 15 (1.43 g, 3.6 mmol) in DMF (10 mL) was introduced. NaH (0.40 g of a 60% dispersion, 12.2 mmol) was then slowly added in one portion, and the reaction mixture was allowed to warm to room temperature over 2 h. The mixture was then cooled to 0 °C, quenched with saturated NH_4Cl, diluted with water, and extracted with EtOAc. The organic layers were washed with brine, dried over $MgSO_4$, filtered, and concentrated. The residue obtained was dissolved in CH_2Cl_2 (21 mL) and treated with TFA (7 mL) for 18 h. Upon concentration, silica gel chromatography using a MeOH/CH_2Cl_2 gradient (1−5% MeOH) provided the desired ketone (0.90 g, 60%). Hydrazine (0.28 mL, 9 mmol) was slowly added to a solution of this ketone (0.76 g, 1.5 mmol) in 1,4-dioxane (15 mL) at room temperature. The reaction was heated to 65 °C for 18 h, concentrated, and purified by column chromatography on silica gel using a EtOAc/hexanes gradient (33 to 100% EtOAc) to provide 3 (0.19 g, 26%). ^{1}H NMR (DMSO-d_6): δ 13.83 (s, 1H, NH), 7.80 (m, 1H), 7.58 (dd, J = 8.5 Hz, 1.7 Hz, 1H), 7.45 (dd, J = 2.45 Hz, 1.3 Hz, 1H), 7.38 (m, 1H), 7.25 (m, 1H), 7.18 (d, J = 7.2 Hz, 1H), 6.37 (d, J = 7.2 Hz, 1H), 4.24 (s, 2H). MS (ESI): 487 (M + H). Anal. Calcd for $C_{21}H_{13}BrClFN_4O_2\cdot0.1H_2O$: C, 51.52; H, 2.72; N, 11.45. Found: C, 51.25, H, 2.63; N, 11.30.

3-[6-Bromo-2-fluoro-3-(1H-pyrazolo[3,4-c]pyridin-3-ylmethyl)phenoxy]-5-chlorobenzonitrile (5). 5 was prepared as described in the general procedure from 3-fluoroisonicotinic acid and ester 14 (10% overall yield). ^{1}H NMR (DMSO-d_6): δ 13.40 (s, 1H, NH), 9.00 (d, J = 1.3 Hz, 1H), 8.20 (d, J = 5.7 Hz, 1H), 7.81 (m, 1H), 7.57 (m, 2H), 7.50 (dd, J = 2.4 Hz, 1.3 Hz, 1H), 7.40 (t, J = 2.0 Hz, 1H), 4.41 (s, 2H). MS (ESI): 457 (M + H). Anal. Calcd for $C_{20}H_{11}BrClFN_4O\cdot0.35H_2O$: C, 51.77; H, 2.54; N, 12.08. Found: C, 51.78; H, 2.25; N, 11.93.

6-Chloro-3-(2,4-difluorophenoxy)pyridazine-4-carboxylic Acid Methyl Ester (20). A solution of (trimethylsilyl)diazomethane (2.0 M in hexane) was slowly added to a 0 °C solution of 3,6-dichloro-4-carboxypyridazine (7.5 g, 39 mmol) in CH_2Cl_2 (30 mL) and MeOH (10 mL) until a persistent yellow color was observed. After addition was complete, the solvents were removed in vacuo. The crude product was purified by column chromatography on silica gel, eluting with an EtOAc/hexane gradient (10−25% EtOAc) to afford 3.89 g (86%) of the methyl ester as a brown oil that solidified on standing. Sodium hydride (1.53 g, 38.27 mmol) was suspended in dry THF (70 mL) under a N_2 atmosphere and cooled, and 2,4-difluorophenol (3.31 mL, 34.94 mmol) was added dropwise via syringe. After the addition was complete, the mixture was stirred for 15 min. Then the cooling bath was removed for 30 min, and finally the solution was again cooled to 0 °C. A solution of the methyl ester (6.89 g, 33.3 mmol) in dry THF (20 mL) was added through a cannula. The resulting mixture was stirred at room temperature overnight and then heated to 50 °C for 3 h. The mixture was cooled to room temperature, and saturated aqueous NH_4Cl (40 mL) was added followed by water (60 mL). The mixture was extracted with EtOAc, dried ($MgSO_4$), filtered, and evaporated. The crude product was purified by SiO_2 chromatography, eluting with an EtOAc/hexane gradient (10−20% EtOAc) to afford 8.15 g (82%) of 20 as a light-yellow oil. ^{1}H NMR ($CDCl_3$): δ 7.94 (s, 1H), 7.27 (m, 1H), 6.95 (m, 1H), 4.02 (s, 3H). MS (ESI): 301 (M + H).

3-(2,4-Difluorophenoxy)pyridazine-4-carboxylic Acid (21). To a solution of **20** (8.15 g, 127.1 mmol) in MeOH (40 mL) was added ammonium formate (8.55 g, 1.1 equiv) followed by 10% palladium on carbon (0.5 g). The mixture was heated to 50 °C for 20 min and then to 60 °C for 35 min. The mixture was cooled to room temperature and filtered. The volatile solvents were evaporated, and the residual material was partitioned between CH$_2$Cl$_2$ (80 mL) and H$_2$O. The CH$_2$Cl$_2$ layer was separated, and the aqueous layer was extracted twice with CH$_2$Cl$_2$ (80 mL). The combined extracts were dried (MgSO$_4$), filtered, and evaporated. The crude product was purified by SiO$_2$ chromatography, eluting with an EtOAc/hexane gradient (10−50% EtOAc) to afford 5.5 g (76%) of the monochloride intermediate as a viscous yellow oil. To a solution of this intermediate (5.0 g, 19.0 mmol) in THF (40 mL) and MeOH (10 mL) was added an aqueous solution of LiOH (21.6 mL, 1.0 M solution). The mixture was stirred for 15 min and concentrated, and the residue was diluted with H$_2$O (25 mL) and THF (20 mL) and then adjusted to pH 2−3 with 10% HCl. The resulting solid was collected by filtration and washed with water (50 mL) and EtOAc (30 mL) to obtain 4.08 g (86%) of **21** as a white powder. ^{1}H NMR (CDCl$_3$): δ 9.21 (d, J = 4.7 Hz, 1H), 8.08 (d, J = 4.7 Hz, 1H), 7.51 (m, 2H), 7.17 (m, 1H). MS (ESI): 253 (M + H).

3-[6-Bromo-2-fluoro-3-(1H-pyrazolo[3,4-c]pyridazin-3-ylmethyl)phenoxy]-5-chlorobenzonitrile (6). 6 was prepared as described in the general procedure from **14** and **21**. ^{1}H NMR (DMSO-d_6): δ 14.25 (s, 1H, NH), 9.08 (d, J = 5.5 Hz, 1H), 8.03 (d, J = 5.5 Hz, 1H), 7.80 (m, 1H), 7.60 (dd, J = 8.5 Hz, 1.7 Hz, 1H), 7.49 (dd, J = 2.3 Hz, 1.2 Hz, 1H), 7.40 (t, J = 2.2 Hz, 1H), 7.33 (t, J = 8.1 Hz, 1H), 4.45 (s, 2H). MS (ESI): 458 (M + H). Anal. Calcd for C$_{19}$H$_{10}$BrClFN$_5$O: C, 49.75; H, 2.20; N, 15.27. Found: C, 49.81; H, 2.16; N, 15.17.

3-[6-Bromo-2-fluoro-3-(1H-pyrazolo[3,4-b]pyrazin-3-ylmethyl)phenoxy]-5-chlorobenzonitrile (7). 1-1′-Carbonyldiimidazole (0.56 g, 3.46 mmol) was added in one portion to a solution of 3-chloropyrazine-2-carboxylic acid (0.50 g, 3.15 mmol) in DMF (5.3 mL). After being heated for 30 min at 50 °C, the solution was cooled to 0 °C and a solution of **15** (1.50 g, 3.46 mmol) in DMF (11 mL) was introduced. Sodium hydride (0.43 g, 60% dispersion in mineral oil, 9.45 mmol) was then slowly added, and the reaction mixture was allowed to warm to room temperature over 2 h. The mixture was then cooled to 0 °C, quenched with saturated NH$_4$Cl, diluted with water, and extracted with EtOAc. The organic layers were washed with brine, dried over magnesium sulfate, filtered, and concentrated. The residue was redissolved in CH$_2$Cl$_2$ (21 mL) and treated with TFA (7 mL) for 18 h. Concentration of the volatile materials in vacuo and silica gel chromatography using a EtOAc/hexanes gradient (5−35% EtOAc) provided 1.0 g of the desired ketone. This material was dissolved in 1,4-dioxane (21 mL), and hydrazine (0.20 mL) was slowly added. The mixture was heated to 60 °C for 1 h, cooled to room temperature, concentrated, and triturated with Et$_2$O to give **7** (0.51 g, 32%). ^{1}H NMR (DMSO-d_6): δ 13.87 (s, 1H, NH), 8.58 (m, 2H), 7.80 (m, 1H), 7.55 (d, J = 8.6 Hz, 1H), 7.47 (s, 1H), 7.33 (t, J = 7.8 Hz, 1H), 4.43 (s, 2H). MS (APCI, negative): 456 (M − H). Anal. Calcd for C$_{19}$H$_{10}$BrClFN$_5$O: C, 49.75; H, 2.20; N, 15.27. Found: C, 49.84; H, 2.23; N, 15.14.

3-Chloro-5-[6-chloro-2-fluoro-3-(1H-pyrazolo[3,4-c]pyridazin-3-ylmethyl)phenoxy]benzonitrile (8). 8 was prepared from 4-chloro-3-(3-chloro-5-cyanophenoxy)-2-fluorophenyl]acetic acid ethyl ester and **21** using the general procedure. ^{1}H NMR (DMSO-d_6): δ 14.29 (s, 1H, NH), 9.09 (d, J = 5.6 Hz, 1H), 8.04 (d, 1H, J = 5.6 Hz), 7.81 (m, 1H), 7.53 (dd, J = 2.3 Hz, 1.2 Hz, 1H), 7.50−7.35 (m, 3H), 4.47 (s, 2H). MS (ESI): 414 (M + H). Anal. Calcd for C$_{19}$H$_{10}$Cl$_2$FN$_5$O: C, 55.09; H, 2.43; N: 16.91. Found: C, 54.99; H, 2.31; N: 16.69.

5-[6-Bromo-2-fluoro-3-(1H-pyrazolo[3,4-c]pyridazin-3-ylmethyl)phenoxy]isophthalonitrile (9). 9 was prepared from 4-bromo-3-(3,5-dicyanophenoxy)-2-fluorophenyl]acetic acid ethyl ester and **21** using the general procedure. ^{1}H NMR (MeOH-d_3): δ 9.04 (d, J = 5.5 Hz, 1H), 8.03 (d, J = 5.5 Hz, 1H), 7.91 (m, 1H), 7.60 (m, 2H), 7.53 (m, 1H), 7.29 (m, 1H), 4.49 (s, 2H). MS (ESI): 449 (M + H).

Anal. Calcd for C$_{20}$H$_{10}$BrFN$_6$O: C, 53.47; H, 2.24; N, 18.71. Found: C, 53.55; H, 2.27; N, 18.65.

3-(4-Bromo-2-nitrophenoxy)-5-methylbenzonitrile (27). Potassium carbonate (8.30 g, 60 mmol) was added to a stirred solution of 3-hydroxy-5-methylbenzonitrile **25** (4.0 g, 30 mmol) and 4-bromo-1-fluoro-2-nitrobenzene **26** (3.7 g, 30 mmol) in DMF (300 mL). The resulting mixture was stirred at room temperature for 48 h. The crude reaction mixture was concentrated under reduced pressure to remove excess DMF. The residue was diluted with EtOAc, washed with water, aqueous 1 M HCl solution, saturated aqueous LiCl solution and dried over MgSO$_4$. Filtration and evaporation of the volatile materials in vacuo provided **27** as a light-brown solid (9.40 g, 94%). ^{1}H NMR (CDCl$_3$): δ 8.14 (d, J = 2.4 Hz, 1H), 7.71 (dd, J = 8.8, 2.4 Hz), 7.26−7.28 (m, 1H), 7.04−7.07 (m, 2H), 6.98 (d, 1H, J = 8.8 Hz), 2.39 (s, 3H).

3-(2-Amino-4-bromophenoxy)-5-methylbenzonitrile (28). Iron powder (6.3 g, 112 mmol), NH$_4$Cl (6.03 g, 112 mmol), and water (180 mL) were added to a solution of **27** (49.4 g, 28.2 mmol) in EtOH (180 mL). The mixture was heated to 100 °C for 4 h, filtered, and evaporated to dryness under reduced pressure. The residue was diluted with EtOAc, washed with saturated aqueous NaHCO$_3$ solution, brine, and dried over MgSO$_4$. Filtration and evaporation of the volatile materials in vacuo provided **28** as an off-white solid (1.50 g, 66%). ^{1}H NMR (CDCl$_3$): δ 7.14−7.16 (m, 1H), 6.96−7.00 (m, 3H), 6.85 (dd, J = 8.5, 2.2 Hz, 1H), 6.72 (d, J = 8.5 Hz, 1H), 2.35 (s, 1H).

[3-Amino-4-(3-cyano-5-methylphenoxy)phenyl]acetic Acid $tert$-Butyl Ester (29). A solution of 2-$tert$-butoxyethylzinc chloride (74.80 mL, 37.40 mmol) in THF was added to a solution of **28** (6.30 g, 20.8 mmol) and bis(tri-$tert$-butylphosphine)palladium (1.60 g, 3.11 mmol) in 1,4-dioxane (200 mL). After being stirred for 20 h, the reaction mixture was filtered and evaporated to dryness under reduced pressure. Column chromatography on silica gel using an EtOAc/hexanes gradient (20−50% EtOAc) provided the desired product **29** as an oil that slowly crystallized on standing (2.30 g, 33%). ^{1}H NMR (CDCl$_3$): δ 7.11−7.14 (m, 1H), 6.98−7.01 (m, 2H), 6.81 (d, J = 8.15 Hz, 1H), 6.77 (d, J = 2.05 Hz, 1H), 6.64 (dd, J = 8.2, 2.1 Hz, 1H), 3.74 (s, 2H), 3.45 (s, 2H), 2.33 (s, 3H), 1.46 (s, 9H).

[3-Bromo-4-(3-cyano-5-methylphenoxy)phenyl]acetic Acid $tert$-Butyl Ester (30). $tert$-Butyl nitrite solution (1.07 mL, 8.15 mmol) was added to a mixture of CuBr$_2$ (1.51 g, 6.79 mmol) and LiBr (1.76 g, 6.79 mmol) in MeCN (90 mL) at 60 °C. After 10 min, a solution of **29** (2.30 g, 6.79 mmol) in MeCN (20 mL) was added. After being stirred at 60 °C for 24 h, the reaction mixture was quenched with aqueous 5% HBr solution (100 mL). The organics were extracted with EtOAc, washed with brine, dried over MgSO$_4$, filtered, and evaporated to dryness in vacuo. Column chromatography on silica gel using an EtOAc/hexanes gradient (10−50% EtOAc) provided the desired product **30** (0.70 g 25%) as an oil. ^{1}H NMR (CDCl$_3$): δ 7.58 (d, J = 2.0 Hz, 1H), 7.22−7.27 (m, 1H), 7.15−7.18 (m, 1H), 6.93−7.05 (m, 3H), 3.53 (s, 2H), 2.35 (s, 3H), 1.47 (s, 9H).

3-[2-Bromo-4-(1H-pyrazolo[3,4-c]pyridazin-3-ylmethyl)phenoxy]-5-methylbenzonitrile (10). Carbonyldiimidazole (0.297 g, 1.83 mmol) was added to a solution of 3-(2,4-difluorophenoxy)pyridazine-4-carboxylic acid (0.462 g, 1.83 mmol) in DMF (8 mL). The contents of the flask were heated at 50 °C under an atmosphere of argon. After 50 min, the reaction mixture was cooled to room temperature and cannulated into a solution of **15** (0.67 g, 1.67 mmol) in DMF (8 mL), followed by the addition of NaH (0.128 g, 5.34 mmol). After 30 min the reaction was quenched by the addition of aqueous 1 M HCl solution. The organics were extracted with EtOAc, washed with brine, dried over MgSO$_4$, filtered, and evaporated to dryness under reduced pressure. The residue was passed through a silica gel plug to provide the intermediate ester as a colorless oil (0.200 g). The ester was dissolved in toluene (1.2 mL) and treated with p-toluenesulfonic acid (0.015 g, 0.08 mmol). The reaction mixture was heated at 150 °C for 4 h and then cooled to room temperature. The crude reaction mixture was quenched by the addition of saturated aqueous NaHCO$_3$ solution. The organics

were extracted with EtOAc, washed with brine, dried over $MgSO_4$, filtered, and evaporated to dryness under reduced pressure. Column chromatography on silica gel using an EtOAc/hexanes gradient (0−40% EtOAc) provided the intermediate ketone as a brown oil (0.081 g, 9% over two steps). ^1H NMR (CDCl$_3$): δ 9.17 (d, J = 4.75 Hz, 1H), 7.82 (d, J = 4.75 Hz, 1H), 6.94−7.06 and 7.17−7.36 (m, 9H), 4.46 (s, 2H), 2.36 (s, 3H). A mixture containing this ketone (0.081 g, 0.15 mmol), *p*-toluenesulfonic acid (0.057 g, 0.30 mmol), and hydrazine monohydrate (17 µL, 0.30mmol) in propan-2-ol was placed under an atmosphere of nitrogen and heated at 80 °C for 14 h. Once cooled, the reaction mixture was treated with 20% aqueous NaCO$_3$ solution. The organics were extracted with EtOAc, washed with brine, dried over MgSO$_4$, filtered, and evaporated in vacuo. Chromatography over silica gel using an EtOAc/hexanes gradient (70−100%) provided **10** as a light-yellow oil (0.019 g, 30%). ^1H NMR (DMSO-d_6): δ 14.3 (s, 1H, NH), 9.09 (d, J = 5.6 Hz, 1H), 8.14 (d, J = 5.6 Hz, 1H), 7.78 (d, J = 2.14 Hz, 1H), 7.42 (m, 1H), 7.38 (dd, J = 8.4 Hz, 2.0 Hz, 1H), 7.20−7.05 (m, 3H), 4.41 (s, 2H), 2.34 (s, 3H). MS (ESI): 420 (M + H). HRMS (ESI) calcd for $C_{20}H_{15}BrN_5O$ (M + H): 420.0460. Found: 420.0462.

HIV-1 Reverse Transcriptase Assay. RNA-dependent DNA polymerase activity was measured using a biotinylated primer oligonucleotide and tritiated dNTP substrate. Newly synthesized DNA was quantified by capturing the biotinylated primer molecules on streptavidin coated scintillation proximity assay (SPA) beads (Amersham). The sequences of the polymerase assay substrate were as follows: 18nt DNA primer, 5′-biotin/GTC CCT GTT CGG GCG CCA-3′; 47nt RNA template, 5′-GGG UCU CUC UGG UUA GAC CAC UCU AGC AGU GGC GCC CGA ACA GGG AC-3′. The biotinylated DNA primer was obtained from the Integrated DNA Technologies Inc., and the RNA template was synthesized by Dharmacon. The DNA polymerase assay (final volume 50 µL) contained 32 nM biotinylated DNA primer, 64 nM RNA substrate, dGTP, dCTP, dTTP (each at 5 µM), 103 nM [^3H]dATP (specific activity = 29 µCi/mmol) in 45 mM Tris-HCl, pH 8.0, 45 mM NaCl, 2.7 mM Mg(CH$_3$COO)$_2$, 0.045% Triton X-100 w/v, 0.9 mM EDTA. The mixtures contained 5 µL of serial compound dilutions in 100% DMSO for IC$_{50}$ determination, and the final concentrations of DMSO were 10%. Reactions were initiated by the addition of 30 µL of the HIV room temperature enzyme (final concentrations of 1−3 nM). Protein concentrations were adjusted to provide linear product formation for at least 30 min of incubation. After incubation at 30 °C for 30 min, the reaction was quenched by addition of 50 µL of 200 mM EDTA (pH 8.0) and 2 mg/mL SA-PVT SPA beads (Amersham, RPNQ0009, reconstituted in 20 mM Tris-HCl, pH 8.0, 100 mM EDTA, and 1% BSA). The beads were left to settle overnight, and the SPA signals were counted in a 96-well top counter-NXT (Packard). IC$_{50}$ values were obtained by sigmoidal regression analysis using GraphPad.

Antiviral Assay. Anti-HIV antiviral activity was assessed using an adaptation of the method of Pauwels et al.[29] The method is based on the ability of compounds to protect HIV-infected T lympho-blastoid cells (MT4 cells) from cell death mediated by the infection. The end point of the assay was calculated as the concentration of compound at which the cell viability of the culture was preserved by 50% ("50% inhibitory concentration", IC$_{50}$). The cell viability of a culture was determined by the uptake of soluble, yellow 3-[4,5-dimethylthiazol-2-yl]-2,5-diphenyltetrazolium bromide (MTT) and its reduction to a purple insoluble formazan salt. After solubilization, spectrophotometric methods were employed to measure the amount of formazan product.

MT4 cells were prepared to be in logarithmic-phase growth and a total of 2×10^6 cells infected with the HXB2-strain of HIV at a multiplicity of 0.0001 infectious units of virus per cell in a total volume of between 200 and 500 µL. The cells were incubated with virus for 1 h at 37 °C before removal of virus. The cells are then washed in 0.01 M phosphate buffered saline, pH 7.2, before being resuspended in culture medium for incubation in culture with serial dilutions of test compound. The culture medium used was RPMI 1640 without phenol red, supplemented with penicillin, strepto-mycin, L-glutamine, and 10% fetal calf serum (GM10).

Test compounds were prepared as 2 mM solutions in dimethyl sulfoxide (DMSO). Four replicate, serial 2-fold dilutions in GM10 were then prepared and 50 µL amounts placed in 96-well plates over a final nanomolar concentration range of 625−1.22. Fifty microliters GM10 and 3.5×10^4 infected cells were then added to each well. Control cultures containing no cells (blank), uninfected cells (100% viability, four replicates), and infected cells without compound (total virus-mediated cell death, four replicates) were also prepared. The cultures were then incubated at 37 °C in a humidified atmosphere of 5% CO$_2$ in air for 5 days.

A fresh solution of 5 mg/mL MTT was prepared in 0.01 M phosphate buffered saline, pH 7.2, and 20 µL added to each culture. The cultures were further incubated as before for 2 h. They were then mixed by pipetting up and down 170 µL of Triton X-100 in acidified isopropanol (10% v/v Triton X-100 in 1:250 mixture of concentrated HCl in isopropanol). When the formazan deposit was fully solubilized by further mixing, the absorbance (OD) of the cultures was measured at 540 and 690 nm wavelength (690 nm readings were used as blanks for artifacts between wells). The percent protection for each treated culture was then calculated from the equation

$$\% \text{ protection} = \{[(\text{OD drug treated cultures}) - (\text{OD untreated virus control cultures})] / [(\text{OD uninfected cultures}) - (\text{OD untreated virus control cultures})]\} \times 100\%$$

The IC$_{50}$ can be obtained from graph plots of percent protection versus log$_{10}$ of the drug concentration.

Antiviral Assay Using Clinical Isolates. Viruses were selected from a panel of clinical isolates available at Monogram Biosciences based on their reduced susceptibility to efavirenz. Compounds were evaluated in the PhenoScreen single cycle antiviral assay at Monogram Biosciences as described previously.[29b]

Crystallization and Structure Determination. Amino acids 1−561 of HIV-1 reverse transcriptase were overexpressed in *E. coli*. Supernatant from disrupted and centrifuged cell pellet was passed over Q Sepharose, heparin HP, C3 HIC, SP Sepharose, and Superdex 200 SEC columns, concentrated to ~12 mg/mL, and stored in 20 mM Tris, pH 7.8, 200 mM NaCl, 1 mM EDTA, 2 mM DTT at −80 °C. An aliquot of thus purified p66/p51 heterodimer reverse transcriptase was mixed with 0.4 mM **6** or **10**. Crystals were grown by sitting drop vapor diffusion over a reservoir of 1.15 M sodium malonate, 50 mM potassium phosphate, pH 7.2, 5% ethylene glycol. Crystals were exchanged into a cryoprotectant of 2 M sodium malonate, 50 mM potassium phosphate, pH 7.5, 5% glycerol, 0.5 M sodium ascorbate including 0.1 mM compound. Crystals were frozen in liquid nitrogen and data collected at the Advanced Light Source beamline 5.0.2 and Stanford Synchrotron Radiation Laboratory beamline 9.2. Data were reduced with HKL2000 and phased using coordinates from an internal structure (i.e., rigid-body refinement in Refmac rather than a full molecular replacement search). Model inspection, building, and refinement were done using PyMOL,[30] COOT,[31] and Refmac.[32,33] Statistics and further details are included in the Supporting Information.

Supporting Information Available: Additional crystallographic information. This material is available free of charge via the Internet at http://pubs.acs.org.

References

(1) Zhou, Z.; Lin, X.; Madura, J. D. HIV-1 RT nonnucleoside inhibitors and their interaction with RT for antiviral drug development. *Infect. Disord.: Drug Targets* **2006**, *6*, 391–413.

(2) Zhang, Z.; Hamatake, R.; Hong, Z. Clinical utility of current NNRTIs and perspectives of new agents in this class under development. *Antiviral Chem. Chemother.* **2004**, *15*, 121–134.

(3) Basavapathruni, A.; Anderson, K. S. Reverse transcription of the HIV-1 pandemic. *FASEB J.* **2007**, *21*, 3795–3808.

(4) Boone, L. Next-generation HIV-1 non-nucleoside reverse transcriptase inhibitors. *Curr. Opin. Invest. Drugs* **2006**, *7*, 128–135.

(5) Balzarini, J. Current status of the non-nucleoside reverse transcriptase inhibitors of human immunodeficiency virus type 1. *Curr. Top. Med. Chem.* **2004**, *4*, 921–944.

(6) Sweeney, Z. K.; Klumpp, K. Improving non-nucleoside reverse transcriptase inhibitors for first-line treatment of HIV infection: the development pipeline and recent clinical data. *Curr. Opin. Drug Discovery Dev.* **2008**, *11*, 458–470.

(7) Xia, Q.; Radzio, J.; erson, K.; Sluis, C. Probing nonnucleoside inhibitor-induced active-site distortion in HIV-1 reverse transcriptase by transient kinetic analyses. *Protein Sci.* **2007**, *16*, 1728–1737.

(8) Jorgensen, W. L.; Ruiz, C.; Tirado, R.; Basavapathruni, A.; Anderson, K. S.; Hamilton, A. D. Computer-aided design of non-nucleoside inhibitors of HIV-1 reverse transcriptase. *Bioorg. Med. Chem. Lett.* **2006**, *16*, 663–667.

(9) Zhou, Z.; Madrid, M.; Evanseck, J.; Madura, J. Effect of a bound non-nucleoside RT inhibitor on the dynamics of wild-type and mutant HIV-1 reverse transcriptase. *J. Am. Chem. Soc.* **2005**, *127*, 17253–17260.

(10) Teague, S. J. Implications of protein flexibility for drug discovery. *Nat. Rev. Drug Discovery* **2003**, *2*, 527–541.

(11) Hopkins, A. L.; Ren, J.; Esnouf, R. M.; Willcox, B. E.; Jones, E. Y.; Ross, C.; Miyasaka, T.; Walker, R. T.; Tanaka, H.; Stammers, D. K.; Stuart, D. I. Complexes of HIV-1 reverse transcriptase with inhibitors of the HEPT series reveal conformational changes relevant to the design of potent non-nucleoside inhibitors. *J. Med. Chem.* **1996**, *39*, 1589–1600.

(12) Hopkins, A. L.; Ren, J.; Milton, J.; Hazen, R. J.; Chan, J. H.; Stuart, D. I.; Stammers, D. K. Design of non-nucleoside inhibitors of HIV-1 reverse transcriptase with improved drug resistance properties. 1. *J. Med. Chem.* **2004**, *47*, 5912–5922.

(13) Ren, J.; Stammers, D. K. HIV reverse transcriptase structures: designing new inhibitors and understanding mechanisms of drug resistance. *Trends Pharmacol. Sci.* **2005**, *26*, 4–7.

(14) Ren, J.; Milton, J.; Weaver, K. L.; Short, S. A.; Stuart, D. I.; Stammers, D. K. Structural basis for the resilience of efavirenz (DMP-266) to drug resistance mutations in HIV-1 reverse transcriptase. *Structure* **2000**, *8*, 1089–1094.

(15) Das, K.; Clark, A. D., Jr.; Lewi, P. J.; Heeres, J.; de Jonge, M. R.; Koymans, L. M.; Vinkers, H. M.; Daeyaert, F.; Ludovici, D. W.; Kukla, M. J.; De, C. B.; Kavash, R. W.; Ho, C. Y.; Ye, H.; Lichtenstein, M. A.; Andries, K.; Pauwels, R.; de Bethune, M. P.; Boyer, P. L.; Clark, P.; Hughes, S. H.; Janssen, P. A.; Arnold, E. Roles of conformational and positional adaptability in structure-based design of TMC125-R165335 (etravirine) and related non-nucleoside reverse transcriptase inhibitors that are highly potent and effective against wild-type and drug-resistant HIV-1 variants. *J. Med. Chem.* **2004**, *47*, 2550–2560.

(16) Cantrell, A. S.; Engelhardt, P.; Hogberg, M.; Jaskunas, S. R.; Johansson, N. G.; Jordan, C. L.; Kangasmetsa, J.; Kinnick, M. D.; Lind, P.; Morin, J. M., Jr.; Muesing, M. A.; Noreen, R.; Oberg, B.; Pranc, P.; Sahlberg, C.; Ternansky, R. J.; Vasileff, R. T.; Vrang, L.; West, S. J.; Zhang, H. Phenethylthiazolylthiourea (PETT) compounds as a new class of HIV-1 reverse transcriptase inhibitors. 2. Synthesis and further structure−activity relationship studies of PETT analogs. *J. Med. Chem.* **1996**, *39*, 4261–4274.

(17) Romines, K.; Freeman, G.; Schaller, L.; Cowan, J.; Gonzales, S.; Tidwell, J.; Andrews, C.; Stammers, D.; Hazen, R.; Ferris, R.; Short, S.; Chan, J.; Boone, L. Structure−activity relationship studies of novel benzophenones leading to the discovery of a potent, next generation HIV nonnucleoside reverse transcriptase inhibitor. *J. Med. Chem.* **2006**, *49*, 727–739.

(18) Girardet, J.-L.; Koh, Y.-H.; De La Rosa, M.; Gunic, E.; Zhang, Z.; Hamatake, R.; Yeh, L. The Discovery of RDEA806, a Potent New HIV NNRTI in Phase 1 Clinical Trials. Presented at the 47th Interscience Conference on Antimicrobial Agents and Chemotherapy, Chicago, IL, 2007; H-1040.

(19) (a) Sweeney, Z. K.; Dunn, J. P.; Li, Y.; Heilek, G.; Dunten, P.; Elworthy, T. R.; Han, X.; Harris, S. F.; Hirschfeld, D. R.; Hogg, J. H.; Huber, W.; Kaiser, A. C.; Kertesz, D. J.; Kim, W.; Mirzadegan, T.; Roepel, M. G.; Saito, Y. D.; Silva, T. M.; Swallow, S.; Tracy, J. L.; Villaseñor, A.; Vora, H.; Zhou, A. S.; Klumpp, K. Discovery and optimization of pyridazinone non-nucleoside inhibitors of HIV-1 reverse transcriptase. *Bioorg. Med. Chem. Lett.* **2008**, *18*, 4352–4354.

(b) Sweeney, Z. K.; Acharya, S.; Briggs, A.; Dunn, J. P.; Elworthy, T. R.; Fretland, J.; Giannetti, A. M.; Heilek, G.; Li, Y.; Kaiser, A. C.; Martin, M.; Saito, Y. D.; Smith, M.; Suh, J. M.; Swallow, S.; Wu, J.; Hang, J. Q.; Zhou, A. S.; Klumpp, K. Discovery of triazolinone non-nucleoside inhibitors of HIV reverse transcriptase. *Bioorg. Med. Chem. Lett.* **2008**, 4348–4351.

(20) Following the completion of this work, a closely related series of annulated pyrazoles was disclosed: Tucker, T. J.; Saggar, S.; Sisko, J. T.; Tynebor, R. M.; Felock, P. J.; Flynn, J. A.; Lai, M.-T.; Liang, Y.; Liu, M.; McGaughey, G.; Miller, M. D.; Moyer, G.; Munshi, V.; Poehnelt, R. A.; Prasad, S.; Sanchez, R.; Torrent, M.; Vacca, J. P.; Williams, T. M.; Wan, B.-L.; Yan, Y. The Design and Synthesis of Diaryl Ether Second Generation HIV-1 Non-Nucleoside Reverse Transcriptase Inhibitors (NNRTIs) with Enhanced Potency versus Key Clinical Mutations. Presented at the 235th National Meeting of the American Chemical Society, New Orleans, LA, 2008; MEDI-174.

(21) Mager, P. P. Evidence of a butterfly-like configuration of structurally diverse allosteric inhibitors of the HIV-1 reverse transcriptase. *Drug Des. Discovery* **1996**, *14*, 241–257.

(22) (a) Ren, J.; Chamberlain, P. P.; Stamp, A.; Short, S. A.; Weaver, K. L.; Romines, K. R.; Hazen, R.; Freeman, A.; Ferris, R. G.; rews, C. W.; Boone, L.; Chan, J. H.; Stammers, D. K. Structural basis for the improved drug resistance profile of new generation benzophenone non-nucleoside HIV-1 reverse transcriptase inhibitors. *J. Med. Chem.* **2008**, *51*, 5000–5008. (b) Rodgers, D. W.; Gamblin, S. J.; Harris, B. A.; Ray, S.; Culp, J. S.; Hellmig, B.; Woolf, D. J.; Debouck, C.; Harrison, S. C. The structure of unliganded reverse transcriptase from the human immunodeficiency virus type 1. *Proc. Natl. Acad. Sci. U.S.A.* **1995**, *92*, 1222–1226.

(23) Huang, H.; Chopra, R.; Verdine, G. L.; Harrison, S. C. Structure of a covalently trapped catalytic complex of HIV-1 reverse transcriptase: implications for drug resistance. *Science* **1998**, *282*, 1669–1675.

(24) Paulini, R.; Muller, K.; Diederich, F. Orthogonal multipolar interactions in structural chemistry and biology. *Angew. Chem., Int. Ed.* **2005**, *44*, 1788–1805.

(25) (a) Toth, G.; Bowers, S. G.; Truong, A. P.; Probst, G. The role and significance of unconventional hydrogen bonds in small molecule recognition by biological receptors of pharmaceutical relevance. *Curr. Pharm. Des.* **2007**, *13*, 3476–3493. (b) Ren, J.; Nichols, C.; Bird, L. E.; Fujiwara, T.; Sugimoto, H.; Stuart, D. I.; Stammers, D. K. Binding of the second generation non-nucleoside inhibitor S-1153 to HIV-1 reverse transcriptase involves extensive main chain hydrogen bonding. *J. Biol. Chem.* **2000**, *275*, 14316–14320.

(26) Das, K.; Lewi, P.; Hughes, S. H.; Arnold, E. Crystallography and the design of anti-AIDS drugs: conformational flexibility and positional adaptability are important in the design of non-nucleoside HIV-1 reverse transcriptase inhibitors. *Prog. Biophys. Mol. Biol.* **2005**, *88*, 209–231.

(27) Hopkins, A. L.; Ren, J.; Tanaka, H.; Baba, M.; Okamato, M.; Stuart, D. I.; Stammers, D. K. Design of MKC-442 (emivirine) analogues with improved activity against drug-resistant HIV mutants. *J. Med. Chem.* **1999**, *42*, 4500–4505.

(28) Das, K.; Bauman, J. D.; Clark, A. D.; Frenkel, Y. V.; Lewi, P. J.; Shatkin, A. J.; Hughes, S. H.; Arnold, E. High-resolution structures of HIV-1 reverse transcriptase/TMC-278 complexes: strategic flexibility explains potency against resistant mutations. *Proc. Natl. Acad. Sci. U.S.A.* **2008**, *105*, 1466–1471.

(29) (a) Pauwels, R.; Balzarini, J.; Baba, M.; Snoeck, R.; Schols, D.; Herdewijn, P.; Desmyter, J.; De, C. E. Rapid and automated tetrazolium-based colorimetric assay for the detection of anti-HIV compounds. *J. Virol. Methods* **1988**, *20*, 309–321. (b) Petropoulos, C. J.; Parkin, N. T.; Limoli, K. L.; Lie, Y. S.; Wrin, T.; Huang, W.; Tian, H.; Smith, D; Winslow, G. A.; Capon, D. J.; Whitcomb, J. M. A novel phenotypic drug susceptibility assay for human immunodeficiency virus type 1. *Antimicrob. Agents Chemother.* **2000**, *44*, 920–928.

(30) DeLano, W. L. The PyMOL Molecular Graphics System. http://www.pymol.org.

(31) Emsley, P.; Cowtan, K. Coot: model-building tools for molecular graphics. *Acta Crystallogr., Sect. D: Biol. Crystallogr.* **2004**, *60*, 2126–2132.

(32) Murshudov, G. N.; Vagin, A. A.; Dodson, E. J. Refinement of macromolecular structures by the maximum-likelihood method. *Acta Crystallogr., Sect. D: Biol. Crystallogr.* **1997**, *53*, 240–255.

(33) The CCP4 suite: programs for protein crystallography. *Acta Crystallogr., Sect. D: Biol. Crystallogr.* **1994**, *50*, 760−763.

JM800527X